

Response to the Topic Editor Comments

Contents:

- 1- Response to the Topic Editor Comments
- 2- The manuscript with tracked changes

1- Response to the review comments

Decision: Publish subject to minor revisions (review by editor) (04 Jun 2018) by Piers Chapman

Thank you very much for your valuable comments and suggestions on this manuscript, entitled “Mixed layer depth variability in the Red Sea”. The comments and suggestions were very helpful in improving the manuscript. The manuscript is modified according to the comments and the changes are given below.

Please note that the manuscript with tracked changes is given in this document itself, after the list of response to the comments.

Comment#1

I think that if you want to use the AVISO data, from which most of the information of the eddy field is derived, then you need to at least point out the deficiencies as detailed by reviewer #2 in section 2.2. I am also not very enthusiastic about some of the description in section 3.3; I don't see any sign in Fig. 7, for example, of eddies that are supposed to exist near 13°, 17° or 26°N, even though this has been reported by others, but there does seem to be a small increase near 15°N in this figure. So I think this section could be shortened and made less important.

Answer:

Part#A: The manuscript is modified accordingly. The number of satellite tracks are relatively lower in the narrow regions like Red Sea and we have mentioned the same in the manuscript also. Even though, the merged satellite product is helpful for a qualitative understanding on the sea level variability in the Red Sea.

[Line number in the clean manuscript: 108-110]

[Line number in the manuscript with tracked changes: 130-132]

Part#B: Agreeing to the Editor comment, the section 3.3 is removed and a shortened form of this section. The description of the impact of eddies in more than 60 lines (in the previous version of the manuscript, lines 235-295) is shortened to just 18 lines (in the revised manuscript, lines 238-255) and merged to section 3.2.

[Line number in the clean manuscript: 238-255]

[Line number in the manuscript with tracked changes: 305-322]

Comment#2

You discuss the MLD climatology in Fig. 3, and stress the importance of the winter minima near 17°N and 25°N. However, from Fig. S3, January showed the fewest samples, so are these minima really significant given that you have 29 latitudinal bands of 0.5° each?

Answer:

The noise in mean MLD for the region around 25N is relatively small (~30+/-9 m) comparing to the difference in MLD values towards northern (~70m) and southern (~50m) grids. So this shallow MLD can be considered.

At 17N, the noise in MLD (44+/-14m) is overlapping with mean MLD of northern (~53m) and southern (~48m) grids. Therefore, additional in-situ data is required to confirm (which may reduce the noise) the observed shallow in this region. So this shallow MLD can be excluded from the manuscript.

The manuscript modified accordingly, to keep the shallow MLD around 25N and exclude the “shallow MLD around 17N”.

[Line number in the clean manuscript: 164-168]

[Line number in the manuscript with tracked changes: 206-210]

Comment#3

I also had some problems with section 3.2, particularly the relationships between the MLD and the forcing functions shown in Fig. 6. In your response to reviewer #2, you said that you have tested these relationships statistically and that they are all significant, yet you don't say this in the paper. So say so, otherwise they are just wiggles in the data.

Answer:

The statistical significance of the correlation values are verified based on T-test following Bretherton et al, (1999)), and the estimated p-value, t-value and the effective degree of freedom show that the correlation values are statistically significant at 95%.

The manuscript modified accordingly.

[Line number in the clean manuscript: 223-226]

[Line number in the manuscript with tracked changes: 289-292]

Comment#4

Finally, in section 3.4, you should reference some of the work in similar areas such as the Gulf of Tehuantepec, where strong winds coming through mountain passes are known to affect mixing.

Answer:

We have included appropriate reference in the manuscript.

[Line number in the clean manuscript: 313-316]

[Line number in the manuscript with tracked changes: 522-525]

Comment#5

Lines 34-37 – suggest you rewrite as: “The Red Sea is an important intermediate water formation region in the world ocean. Red Sea Outflow Water (RSOW), formed mainly due to open-ocean convection in the northern Red Sea (Sofianos and Johns, 2002), propagates through Bab-el-Mandab to the Gulf of Aden (A&S 2007) and later spreads to the Indian Ocean. Its signature reaches.....”

Answer:

The manuscript modified accordingly.

[Line number in the clean manuscript: 34-38]

[Line number in the manuscript with tracked changes: 35-39]

Comment#6

Lines 49-50 – suggest “The Red Sea has been investigated for many years with an emphasis on its different physical features, but there has been no detailed investigation on MLD variability, apart from a few studies addressing the hydrography....”

Answer:

The manuscript modified accordingly.

[Line number in the clean manuscript: 49-52]

[Line number in the manuscript with tracked changes: 58-61]

Comment#7

Line 64: End the sentence after “is the main source.” and delete “with larger number of profiles.”

Answer:

The manuscript modified accordingly.

[Line number in the clean manuscript: 64]

[Line number in the manuscript with tracked changes: 73]

Comment#8

Lines 125-127 – delete the last sentence of this paragraph (“This method first identifies....”) as it merely repeats what you have said already.

Answer:

The manuscript modified accordingly.

[Line number in the clean manuscript: 128]

[Line number in the manuscript with tracked changes: 158]

Comment#9

Lines 162-163 – suggest you talk about the region between 14°-21°N as a whole, rather than splitting it up (see my comment about MLD climatology above). Is a change from 48 \pm 9 to 44 \pm 14 really significant? Should the reference in line 162 be to Yao et al 2014b?

Answer:

Part#A: *The manuscript modified accordingly. As suggested in the comment, the noise in mean MLD around 17°N is significantly high. Therefore, the text is corrected accordingly and this shallow region is not considered.*

[Line number in the clean manuscript: 164-168]

[Line number in the manuscript with tracked changes: 206-210]

Part#B: The reference is corrected as Yao et al 2014b.

[Line number in the clean manuscript: 163]

[Line number in the manuscript with tracked changes: 205]

2- The manuscript with tracked changes

1 **Mixed layer depth variability in the Red Sea**

2 Cheriyei P. Abdulla^{1*}, Mohammed A. Alsaafani^{1,2}, Turki M. Alraddadi¹, and Alaa M. Albarakati¹

3 ¹Department of Marine Physics, Faculty of Marine Sciences, King Abdulaziz University, Jeddah, Saudi Arabia.

4 ²Department of Earth & Environmental Sciences, Faculty of Science, Sana'a University, Yemen.

5

6 *Correspondence to:* Cheriyei P. Abdulla (acp@stu.kau.edu.sa)

7 **Abstract**

8 For the first time, a monthly climatology of mixed layer depth (MLD) in the Red Sea has been derived
9 based on temperature profiles. The general pattern of MLD variability is clearly visible in the Red Sea,
10 with deep MLDs during winter and shallow MLDs during summer. Transitional MLDs have been found
11 during the spring and fall. Northern end of the Red Sea experienced deeper mixing and higher MLD,
12 associated with the winter cooling of the high-saline surface waters. Further, the region north of 19°N
13 experienced deep mixed layers, irrespective of the season. Wind stress plays a major role in the MLD
14 variability of the southern Red Sea, while net heat flux and evaporation are the dominating factors in the
15 central and northern Red Sea regions. Ocean eddies and Tokar gap winds significantly alters the MLD
16 structure in the Red Sea. The dynamics associated with the Tokar gap winds leads to a difference of more
17 than 20 m in the average MLD between the north and south of the Tokar axis.

18 **Keywords:** Mixed layer depth, Red Sea, Eddies, Tokar gap winds, Air-Sea interaction.

Deleted: °

20 1 Introduction

21 The surface mixed layer is a striking and universal feature of the open ocean where the turbulence
22 associated with various physical processes leads to the formation of a quasi-homogeneous layer with
23 nearly uniform properties. The thickness of this layer, often named mixed layer depth (MLD), is one of
24 the most important oceanographic parameters, as this layer directly communicates and exchanges energy
25 with the atmosphere and therefore has a strong impact on the distribution of heat (Chen et al., 1994),
26 ocean biology (Polovina et al., 1995) and near-surface acoustic propagation (Sutton et al., 2014). Heat
27 and fresh-water exchanges at the air-sea interface and wind stress are the primary forces behind turbulent
28 mixing. The loss of heat and/or freshwater from the ocean surface can weaken the stratification and
29 enhance the mixing. Similarly, a gain in heat and/or freshwater can strengthen the stratification and reduce
30 the mixing. The shear and stirring generated by the wind stress enhance the vertical mixing and play a
31 major role in controlling the deepening of the oceanic mixed layer. Further, the stirring associated with
32 turbulent eddies predominantly changes the mixing process, mainly along the isopycnal surfaces where
33 stirring may occur with minimum energy (de Boyer Montegut et al., 2004; Hausmann et al., 2017; Kara
34 et al., 2003).

35 The Red Sea is an important intermediate water formation region in the world ocean. Red Sea Outflow
36 Water (RSOW), formed mainly due to open ocean convection in the northern Red Sea (Sofianos and
37 Johns, 2002), propagates through Bab-el-Mandab to the Gulf of Aden (Alsaafani and Shenoi, 2007) and
38 later spreads to the Indian Ocean. Its signature reaches into the south Indian Ocean about 6000 km away
39 from the source (Beal et al., 2000). The Red Sea is surrounded by extremely hot arid lands and has a
40 relatively strong evaporation rate (2 m yr^{-1}) with nearly zero precipitation (Albarakati and Ahmad, 2013;
41 Bower and Farrar, 2015; Sofianos et al., 2002). This region experiences strong seasonality in its
42 atmospheric forcing and buoyancy. These characteristics, along with the lack of river input, make the Red
43 Sea one of the hottest and most saline ocean basin in the world. The narrow and semi-enclosed nature of
44 the basin, the presence of multiple eddies, strong evaporation, lack of river input and very weak
45 precipitation, seasonally reversing winds, etc. lead to complex dynamical processes in the Red Sea
46 (Aboobacker et al., 2016; Yao et al., 2014a, 2014b; Zhai and Bower, 2013; Zhan et al., 2014).

Deleted: It is one of the important intermediate water formation regions in the world (Red Sea Outflow Water, RSOW), formed mainly due to the open ocean convection in the northern Red Sea (Sofianos and Johns, 2002), which propagates through Bab-el-Mandab to the Gulf of Aden (Alsaafani and Shenoi, 2007) and later spreads to the Indian Ocean, whose signature reaches into the south Indian Ocean about 6000 km away from the source (Beal et al., 2000).

55 The increase in number temperature and salinity profiles in recent years enhanced the study of MLD
56 structure and its variability, both globally (de Boyer Montegut et al., 2004; Kara et al., 2003; Lorbacher
57 et al., 2006) and regionally (Abdulla et al., 2016; D’Ortenzio et al., 2005; Keerthi et al., 2012, 2016; Zeng
58 and Wang, 2017). The Red Sea has been investigated for many years with an emphasis on its different
59 physical features, but there has been no detailed investigation on MLD variability, apart from a few
60 studies addressing the hydrography and vertical mixing of localized areas (Alsaafani and Shenoi, 2004;
61 Bower and Farrar, 2015; Carlson et al., 2014; Yao et al., 2014b).
62 In this work, an MLD climatology is produced for the first time based on in situ observations. Further,
63 the roles of atmospheric forces and oceanic eddies on the changes of the MLD have been investigated.
64 The following sections are arranged as: Sect. 2 describes the datasets used and methodology. The
65 subsequent sections discuss the observed MLD variability in the Red Sea, the role of the major forces on
66 the MLD variability, and the influence of Tokar gap winds. The main conclusions of the present work are
67 given in the final section.

68 2 Data and methods

69 2.1 Datasets

70 Temperature and salinity profiles from different sources are collected, which are measured using CTD
71 (conductivity-temperature-density profiler), PFL (autonomous profiling floats including ARGO floats),
72 XBT (expendable-bathy-thermograph) and MBT (mechanical-bathy-thermograph). The World Ocean
73 Database (<https://www.nodc.noaa.gov/OC5/SELECT/dbsearch/dbsearch.html>) is the main source. Apart
74 from this, data from Coriolis data center ([http://www.coriolis.eu.org/Data-Products/Data-Delivery/Data-
75 selection](http://www.coriolis.eu.org/Data-Products/Data-Delivery/Data-selection)) and several cruises conducted by individual institutions are also used in this analysis. The
76 bathythermograph profiles were depth-corrected based on Cheng et al., (2014). A total 13,891 temperature
77 profiles were made for the Red Sea (approximately 14 % of these profiles have salinity measurements)
78 from 1934 to 2017.

Deleted: The Red Sea has been investigated for many years with an emphasis on its different physical features. But, no detailed investigation on MLD variability has been documented so far in the Red Sea, except few studies addressing the hydrography and vertical mixing of localized areas (Alsaafani and Shenoi, 2004; Bower and Farrar, 2015; Carlson et al., 2014; Yao et al., 2014b). ¶

Deleted: (Sect. 3)

Deleted: (Sect. 4)

Deleted: the impact of eddies on MLD changes (Sect. 5)

Deleted: (Sect. 6)

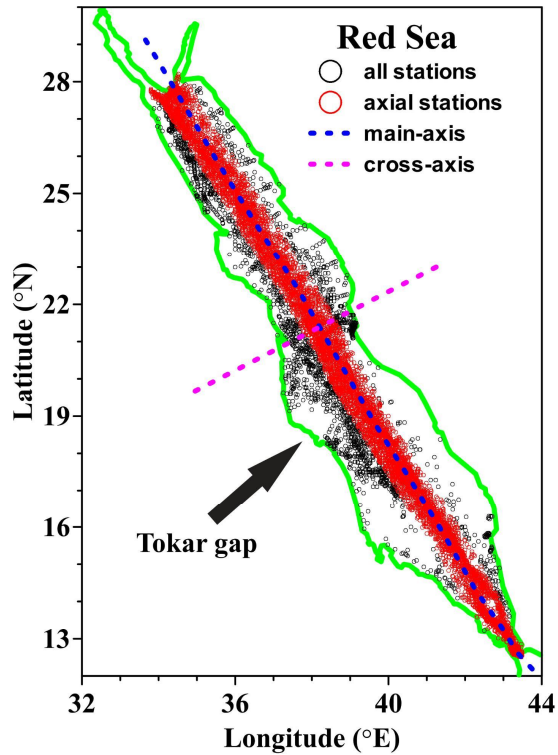
Deleted: with larger number of profiles

90 These profiles are quality checked according to the procedure given in Boyer and Levitus (1994). In the
91 duplicate check, all the profiles within a 1 km radius and taken on the same day are considered duplicates
92 and are removed from the main dataset. The levels in the profile with large inversions in temperature
93 (inversion $\geq 0.3^{\circ}\text{C}$) are flagged and removed. If three or more inversions are present, then the entire
94 profile is removed. The levels with extreme gradients $\geq 0.7^{\circ}\text{C}$ are also removed from the profile. Since
95 the present work is more focused on the changes in the upper layer of the ocean (from the surface to a
96 150 m depth), profiles with low resolutions in the upper layers are removed. Almost 50 % of the profiles
97 have resolutions of <5 m, while 7 % of the profiles have poor resolutions (resolutions of > 25 m).

98 Out of the total of 13,891 profiles analysed, 11,212 profiles passed the quality check from CTD (690),
99 PFL (1385), XBT (5507) and MBT (3630), and the spread is shown in Fig. 1. More than 80 % of these
100 profiles are positioned along the middle of the Red Sea, with a sufficient number of profiles for each
101 month (Fig. S1). The yearly and monthly distributions of the temperature profiles lie along the middle of
102 the Red Sea and are given in the supplementary material (Fig. S2-S3). As part of the quality check, 2679
103 profiles were removed from the main dataset. A total of 2063 salinity profiles are available for the entire
104 Red Sea (Fig. S4). MLD is estimated based on the temperature profiles due to the increased number and
105 sufficient monthly coverage comparing to that of salinity. The distribution of the temperature profiles
106 used in this analysis is shown in Fig. 1.

Deleted: °

Deleted: °



109

110 **Figure 1.** The locations of temperature profiles in the Red Sea. Black circles denote all available profiles,
 111 while red circles denote the profiles close to the main-axis that used for climatology calculation. The blue
 112 (magenta) dashed line indicate main-axis (cross-axis) of the Red Sea.

113 The monthly mean values of heat fluxes and wind stress data are provided by Tropflux at a $1^\circ \times 1^\circ$ spatial
 114 resolution for the period 1979-2016, which are used to check the influence on MLD variability
 115 (http://www.incois.gov.in/tropflux_datasets/data/monthly/). Tropflux captures better variability and less
 116 bias than the other available fluxes and wind stress products (Praveen Kumar et al., 2012, 2013). Since
 117 evaporation is not provided by Tropflux, the monthly mean values of evaporation from OAflux (from

118 1979 to 2016 and $1^{\circ} \times 1^{\circ}$ spatial resolution) are used
119 (ftp://ftp.whoi.edu/pub/science/oaflux/data_v3/monthly/evaporation/). The TRMM (Tropical rainfall
120 measuring mission, <https://pmm.nasa.gov/data-access/downloads/trmm>) satellite provided the
121 precipitation information for every $0.25^{\circ} \times 0.25^{\circ}$ grid and 3-hourly to monthly time scale from 1997 to
122 2016 (TRMM monthly 3B43_V7 product is used). Monthly climatology of heat flux, evaporation,
123 precipitation and wind stress are calculated. The period of precipitation data used for climatology
124 calculation is shorter than other parameters. The present analysis is focusing on the seasonal timescale,
125 and therefore, shorter data period will not significantly affect the results.

126 The daily sea level anomaly (SLA) maps are provided by AVISO (www.aviso.oceanobs.com). These data
127 are the merged product of satellite estimates from TOPEX/Poseidon, Jason-1, ERS-1/2, and Envisat and
128 are globally available with spatial resolution of $0.25^{\circ} \times 0.25^{\circ}$ from the year 1992 to present (Ducet et al.,
129 2000; LaTraon and Dibarboure, 1999). The SLA maps are used to describe the eddy distribution in the
130 Red Sea. The merged data from all satellite estimates provides a general picture of SLA variability and
131 the eddy distribution in the Red Sea, even though the number of satellite tracks passing through the narrow
132 regions like Red Sea are relatively lower than the major ocean basins. Climate Forecast System Reanalysis
133 (CFSR, <https://rda.ucar.edu/datasets/ds093.1/#!access>) provided hourly wind product from 1979 to 2010
134 at a resolution of $0.312^{\circ} \times 0.312^{\circ}$ grid (Saha et al., 2010), which is validated in the Red Sea (Aboobacker
135 et al., 2016; Shanas et al., 2017). CFSR hourly wind at 10 m above the surface is used to study the Tokar
136 gap winds.

137 2.2 Methods

138 The MLD can be estimated based on different methods. The Fig.2 shows a sample temperature profile
139 collected on 19th January 2015 from Red Sea (24.9°N , 35.18°E), with short-range gradients within the
140 mixed layer. This gradient could rise from instrumental errors or turbulence in the upper layer. The
141 curvature method (Lorbacher et al., 2006) identified MLD at 32 m, due to the presence of a short-range
142 gradient at this depth. The threshold method (de Boyer Montegut et al., 2004) detected MLD at 130 m
143 (threshold = 0.2°C), while the segment method (Abdulla et al., 2016) identified MLD at 120 m. The

Deleted: for every $0.25^{\circ} \times 0.25^{\circ}$ grid from

Deleted: at every $0.312^{\circ} \times 0.312^{\circ}$ grid
(<https://rda.ucar.edu/datasets/ds093.1/#!access>)

Deleted: which is validated in the Red Sea by Aboobacker et al.,
(2016).

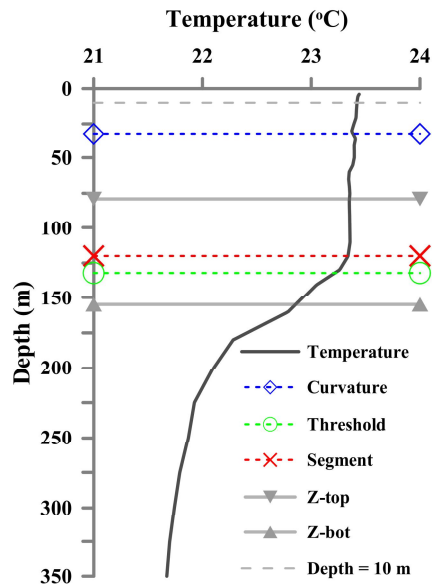
Deleted: °

Deleted: °

Deleted: °

152 segment method based MLD could be considered as a reliable estimate comparing to both curvature
 153 (underestimation) and threshold method (overestimation). The segment method first identifies the portion
 154 of the profile with significant inhomogeneity where the transition from a homogeneous layer to
 155 inhomogeneous layer occurs. Then, this portion of the profile is analyzed to determine the MLD (detailed
 156 procedure of the estimation technique is given Abdulla et al., 2016). In the present study, MLD is
 157 estimated based on the segment method, which is found to be less sensitive to short-range disturbances
 158 within the mixed layer (Abdulla et al., 2016).

Deleted: This method first identifies the portion of the profile (segment) where the transition from a homogeneous layer to inhomogeneous layer occurs. Then, this segment is analyzed to determine the MLD.



160
 161 **Figure 2.** The MLD estimated for a sample temperature profile based on curvature, threshold, and
 162 segment methods. The Z-top and Z-bot respectively represent the top and bottom ends of the portion of
 163 the profile with significant inhomogeneity.

168 The availability of profiles is denser along the middle of Red Sea during all months. The present analysis
169 is performed for the profiles that fall within 0.5 degrees to the east and west of the main axis that, running
170 along almost the middle of the Red Sea (hereafter called the “main axis”), has the advantage of a sufficient
171 number of profiles for every month. The main axis of the Red Sea is inclined to the west, with respect to
172 true north, by ~30 degrees. For this reason, instead of zonally averaging, the climatology is calculated by
173 averaging the MLDs in an inclined direction parallel to the “cross-axis” (Fig. 1). The MLD is estimated
174 for the individual profiles, and then, the monthly climatology is calculated every 0.5° from south to north
175 (13°N to 27.5°N).

Deleted:
Deleted:

176 The heat flux, evaporation, precipitation and wind stress are interpolated to 0.5°x0.5° spatial grid to match
177 with MLD climatology with the help of climate data operator (CDO) tool available at
178 <http://www.mpimet.mpg.de/cdo>. The change in surface water buoyancy forces is calculated following
179 (Turner, 1973)

$$180 \quad B_0 = (C_p^{-1} g \alpha \rho_0^{-1} Q_{net}) + (-1 * g \beta s (E - P)) = B_{0T} + B_{0H} \quad (1)$$

181 where C_p = water heat capacity, g = acceleration due to gravity, α =thermal expansion coefficient, ρ_0 =
182 density of surface water, Q_{net} = net heat flux at the sea surface, β = haline contraction coefficient, s =salinity
183 of surface water, E = evaporation rate, and P = precipitation. In Eq. (1), B_{0T} and B_{0H} , respectively, represent
184 the thermal and haline components of the buoyancy force. For ease of explanation, the Red Sea is divided
185 into southern (13°N-18°N), central (18°N-23°N) and northern (23°N-28°N) regions and the seasons
186 defined as winter (Dec-Feb), spring (Mar-Apr), summer (May-Aug) and fall (Sep-Nov).

Deleted: °
Deleted: °
Deleted: °
Deleted: °
Deleted: °
Deleted: °

187 3 Results and discussion

188 3.1 MLD variability in the Red Sea

189 The Red Sea exhibits strong seasonal changes in its MLD, with deeper mixed layers during the winter
190 and shallower ones during the summer, with gradual changes from deeper to shallower and vice versa in
191 the transitional months. A Hovmoller diagram of the monthly MLD climatology is presented in Fig. 3.

200 The deepest MLD is observed in February and the shallowest during May-Jun. A significant annual
201 variability is observed in the Red Sea. The maximum value of climatological mean MLD is observed in
202 February at the northern Red Sea while the minimum noticed at various instances, especially during
203 summer months. The MLD of individual profiles in the northern Red Sea has a wide range values from
204 40 to 120 m mainly due to the presence of active convection process, while some of the profiles show
205 MLD deeper than 150 m in consistence with [Yao et al., \(2014b\)](#).

Deleted: Yao et al., (2014)

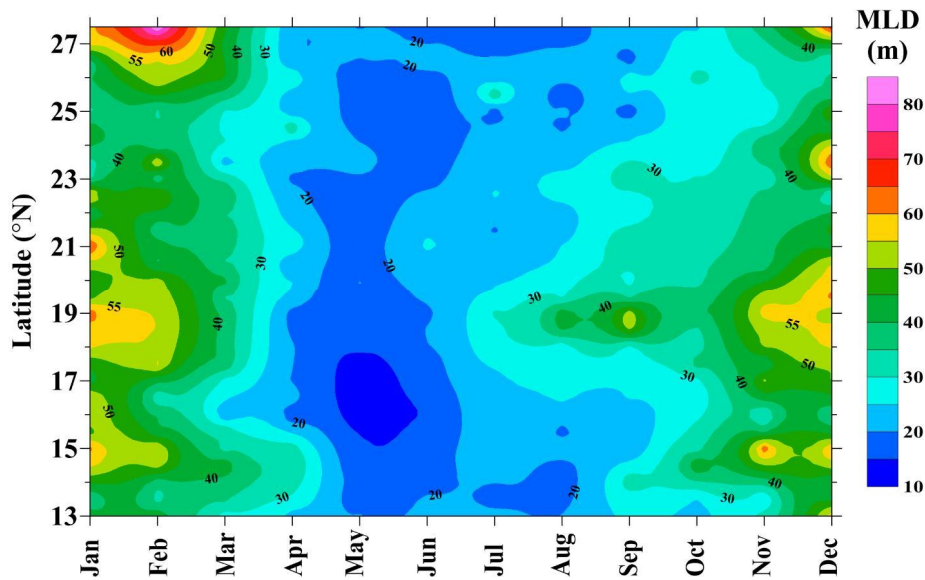
206 In addition, the southern central Red Sea (14°N-21°N) also experienced deeper MLDs during winter. The
207 observed shallow MLD patches are not considered because the noise in MLD (~44±14m) is overlapping
208 with mean MLD of northern (~53m) and southern (~48m) grids. The observed noise around 25°N is
209 relatively small (~30±9 m) comparing to the difference in MLD values towards northern (~70m) and
210 southern (~50m) latitudes, and hence this is considered as a shallow MLD region.

Deleted: +/-

Deleted: +/-

211 During July to September, the region around 19°N experienced a deeper mixed layer in contrast with the
212 general pattern of summer shoaling over the entire Red Sea. The deepening of the MLD begins in October
213 throughout the Red Sea. The winter cooling and associated convection strengthens by December, with
214 an average MLD>50 m, which intensifies by January and persists throughout February.

Deleted: Apart from the northern deep convection region, the south-central Red Sea between 18°N-21°N (53±5 m) and 14°N-16°N (48±9 m) also experienced deeper MLDs during the winter, which is separated by a shallower MLD around 17°N (44±14 m). During July to September, the region around 19°N experienced a deeper mixed layer in contrast with the general pattern of summer shoaling over the entire Red Sea. The deepening of the MLD begins in October throughout the Red Sea. The winter cooling and its associated convection strengthen by December, with an average MLD>50 m. Compared to other parts of the Red Sea, during November and December, relatively shallower MLDs were witnessed at approximately 16°N-17°N, and 24.5°N-26.5°N. The winter deepening of the MLDs intensifies by January and continues throughout February. The area between 24°N and 27°N shows a relatively shallow MLD almost throughout the year, especially during winter. ¶



237

238 **Figure 3.** Hovmöller diagram of the MLD climatology along the axis of Red Sea.

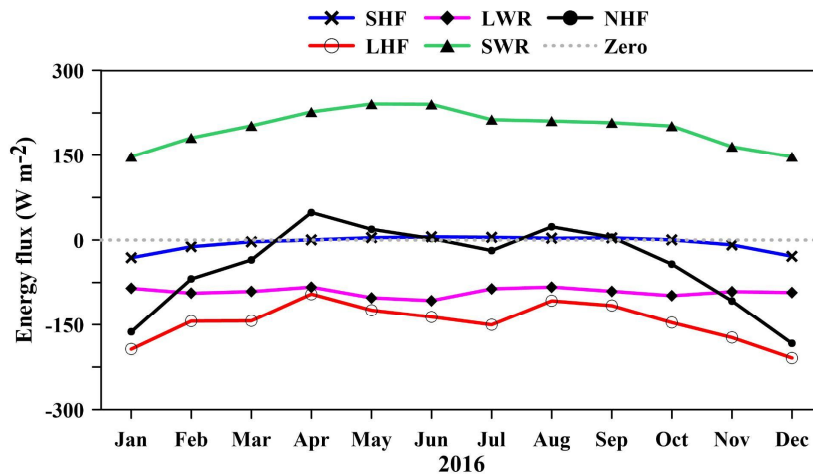
239 The mixed layer starts to shoal gradually by the end of February, and the MLDs of most areas decreases
 240 to 20 ± 7 m by April. Summer shoaling is comparatively stronger in the 15°N - 18°N latitude band, and the
 241 detected mean MLD is < 15 m. Individual observations revealed that many profiles have MLDs < 5 m.
 242 In general, the shallow mixed layers are predominant from April to September, while this prevails until
 243 October in the far north. In the south-central Red Sea, the shallow mixed layer exists for only a short
 244 period, from April to June.

245 **3.2 Major forces controlling the MLD variability**

246 MLD is directly influenced by changes in the net heat flux (NHF), fresh-water flux (E-P) and wind stress.
 247 The different terms that contribute to NHF are given in Fig. 4 for a sample year 2016 in the central Red
 248 Sea. On an annual average basis, the incoming shortwave radiation (SWR, 202 W m^{-2} , positive

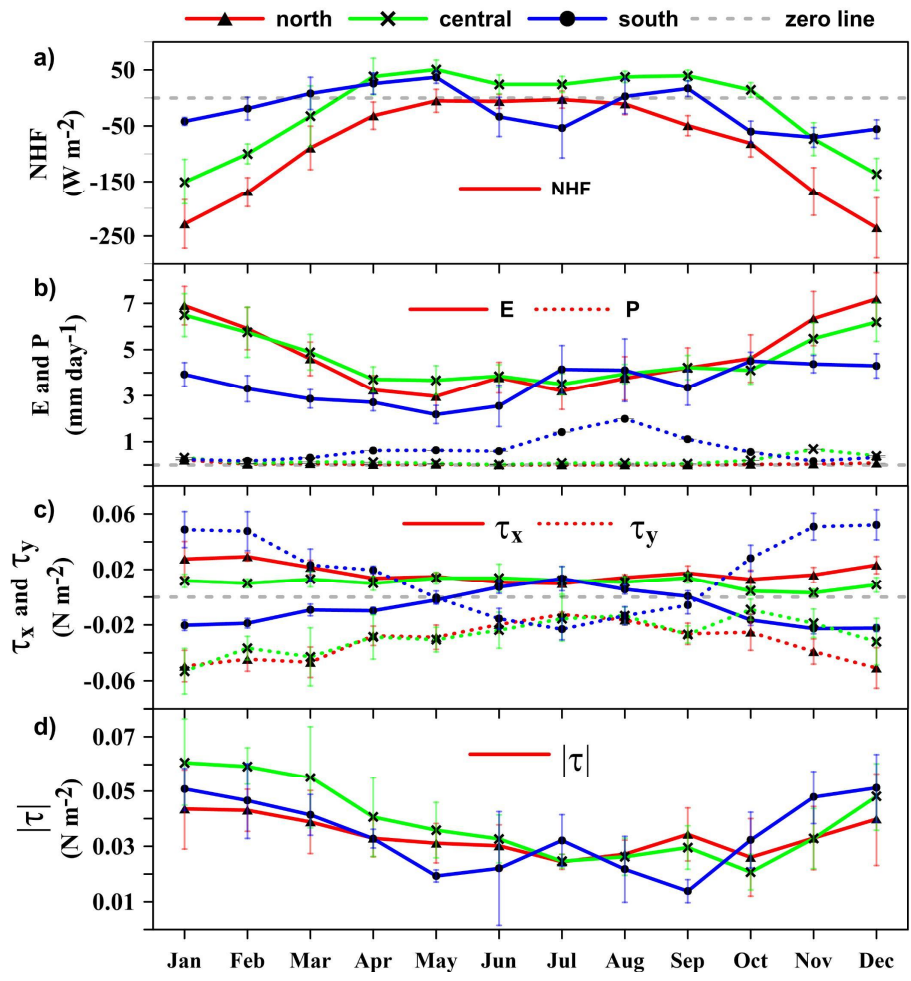
Deleted: +/-
 Deleted: °
 Deleted: °

252 downward) is mainly balanced by LHF (latent heat flux, -126 W m^{-2}) and LWR (long wave radiation, $-$
 253 83 W m^{-2}), while the SHF (sensible heat flux) is only -4 W m^{-2} . The net heat loss in the central Red Sea
 254 is 11 W m^{-2} . Both the LHF and LWR are gradually increasing towards the northern Red Sea. The monthly
 255 climatology of the NHF in the northern, central and southern Red Sea are given in Fig. 5a. Heat loss rises
 256 above 200 W m^{-2} during December-January in the northern Red Sea, with a maximum of $\sim 250 \text{ W m}^{-2}$ at
 257 the northern end of the sea in December. The annual mean of NHF is negative (heat loss) across the Red
 258 Sea, except for isolated locations in the southern Red Sea with trivial heat gain (figure not shown). The
 259 thermal components of the buoyancy forces calculated based on Eq. (1) show that the heat flux support
 260 mixing through buoyancy loss in the northern and central Red Sea during the winter, while it opposes
 261 vertical mixing due to buoyancy gain during summer. In the southern Red Sea, the effect of heat flux is
 262 relatively weak.



263
 264 **Figure 4.** Time series of heat flux components (incoming shortwave radiation (SWR), long wave
 265 radiation (LWR), latent heat flux (LHF), sensible heat flux (SHF) and net heat flux (NHF)) for the year
 266 2016 in the central Red Sea.

267 The evaporation rate in the Red Sea gradually increases from south to north (Fig. 5b). The central and
268 northern Red Sea have higher evaporations during the winter ($\sim 6 \text{ mm day}^{-1}$) and moderate evaporations
269 ($\sim 3 \text{ mm day}^{-1}$) during the summer. Evaporation shows weak seasonality in the southern Red Sea.
270 Precipitation in the southern region is higher than those of the other areas of Red Sea, with maximum
271 rainfall during July-September (Fig. 5b). The changes in buoyancy forces corresponding to fresh-water
272 flux (haline component) are estimated based on Eq. (1), which shows that the changes support vertical
273 mixing throughout the year and over the entire Red Sea. The thermal component is relatively higher than
274 the haline component, and the net buoyancy flux follows a more or less similar pattern of thermal
275 buoyancy flux all along the Red Sea (figure not shown). The observed variability of the above-discussed
276 parameters is consistent with findings from earlier studies (Albarakati and Ahmad, 2013; Sofianos et al.,
277 2002; Tragou et al., 1999).

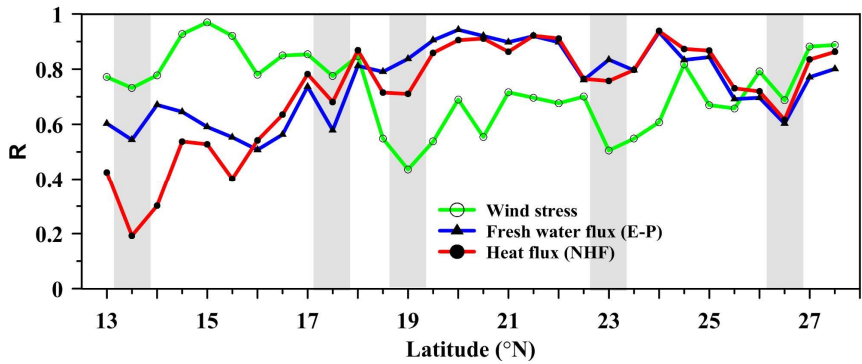


278

279 **Figure 5.** Monthly climatology of a) NHF, b) evaporation and precipitation, c) eastward (τ_x) and
 280 northward (τ_y) component of wind-stress, and d) magnitude of the wind stress ($|\tau|$). South, central and
 281 north regions are represented by the changes at 14°N, 21°N and 27°N.

282 The pattern of wind stress in the Red Sea is significantly different from the other parameters. The wind
 283 stress is strong during the winter, leading to enhanced turbulence and mixing, while it is weak during the
 284 summer, resulting in a shallower mixed layer (Fig. 5c,d). Apart from that, strong surface winds blow to
 285 the Red Sea through the Tokar gap at approximately 19°N in July and August.

Deleted: °



286
 287 **Figure 6.** Correlation between major forces and MLD. Shaded regions represent locations of coinciding
 288 drops in correlation.

289 The correlations between MLDs and forcing factors are given in Fig. 6. The statistical significance of the
 290 correlation values are verified based on t-test following (Bretherton et al., 1999), and the estimated p-
 291 value, t-value and the effective degree of freedom show that the correlation values are statistically
 292 significant at 95%. The wind stress and E-P are positively correlated with MLD while the NHF is
 293 negatively correlated since as NHF (into the ocean) increases, MLD decreases. For simplicity of the figure
 294 (Fig. 6), the correlation values of all parameters are presented as positive. NHF and E-P are well correlated
 295 (>0.8) with MLD in the central and northern Red Sea, and weakly correlated in the south. Wind stress has
 296 a higher correlation (>0.8) to the south, while it is relatively weakly correlated in the central and northern
 297 Red Sea. Toward the northern end, the wind stress gradually achieves a higher correlation.

299 The results from Fig. 5 and 6 indicate that the MLD variability of the Red Sea is dominated by wind stress
300 in the southern part, NHF (heat flux) and evaporation play a major role in the central region, while all the
301 three are influencing in the northern region. Remarkably, for all the above-discussed parameters,
302 coinciding drops are observed in the correlations at approximately 13.5°N, 17.5°N, 19°N, 23°N, and
303 26.5°N, which indicate the impact of additional forces like eddies and currents in regulating the MLD
304 variability of the region.

305 Earlier studies have proved that the upper ocean is efficiently re-stratified by the ocean eddies which may
306 significantly change the MLD. The resultant effect of eddy is largely dependent on the eddy amplitude.
307 The mixing intensity is largest at the center of eddy and decays on average with increasing radial distance
308 (Dewar, 1986; Fox-Kemper et al., 2008; Hausmann et al., 2017; Smith and Marshall, 2009). The observed
309 results show that the mixing associated with eddies is dominating over the existing effect of wind stress
310 and heat flux. CE diminishes mixing through upwelling of the subsurface water while AE enhances
311 mixing through downwelling of the surface water (de Boyer Montegut et al., 2004; Chelton et al., 2004,
312 2011; Dewar, 1986; Hausmann et al., 2017).

313 Satellite altimetry maps revealed the presence of multiple eddies in the Red Sea which are often confined
314 to specific latitude bands (Clifford et al., 1997; Johns et al., 1999; Quadfasel and Baudner, 1993; Sofianos
315 and Johns, 2007). Analyzing the SLA maps from 1992 to 2012, Zhan et al., (2014) reported the presence
316 of multiple eddies with both polarities in the Red Sea. The number of identified eddies peaked at
317 approximately 19.5°N and 23.5°N. The upwelling proxy constructed using MODIS SST in the northern
318 Red Sea shows the presence of frequent upwelling events at approximately 26.5°N almost every year
319 (Papadopoulos et al., 2015) indicating the presence of cyclonic eddy. The extent and time of the upwelling
320 vary from year to year. In summary, significantly large number of eddies are noticed around 19.5°N,
321 23.5°N and 26.5°N, which could be the possible reason for coinciding drops in the correlation around
322 19°N, 23°N and 26.5°N.

323 The Red Sea is very narrow at 13.5°N. Moreover, complex dynamics occur in this region associated with
324 surface and subsurface currents in the strait between the Red Sea and the Gulf of Aden. The complexity
325 of this region prevents linking the MLD variability directly to atmospheric forcing or eddies. The region

Deleted: °
Deleted: °
Deleted: °
Deleted: °
Deleted: °
Deleted: . These drops are discussed in the following section.

Deleted: °

Deleted: °

Deleted: °

Deleted: °

Deleted: °

at approximately 17.5°N is between the two eddy-driven downwelling zones at approximately 15°N and 19°N (Fig. 3). Mass conservation requires upwelling to replace the downwelling water. The MLD climatology shows shallow mixed layers throughout the year at 17.5°N, which could be due to possible upwelling. Further investigation is required to unveil the dynamics associated with this region.

3.3 Influence of Tokar gap winds during the summer

The Tokar gap is one of the largest gaps in the high orography located on the African coast of the Red Sea, near 19°N. Strong winds are funneled to the Red Sea through this gap which last for few days to weeks. Figure 7a shows the u-component of CFSR hourly surface wind at the Tokar region from 1996 to 2006. From the figure, it shows that the strong wind events occur during summer every year while the intensity and duration of the event varies from year to year. Tokar gap winds frequently attain a speed of 15 m s⁻¹. Previous research also show similar results (Jiang et al., 2009; Ralston et al., 2013; Zhai and Bower, 2013). Zhai and Bower (2013) reported that wind speed may reach 20 to 25m s⁻¹ based on ship-based observations. Figure 7b show that the onset of 2001 Tokar event was on 20th July and continued till 20th August, where the maximum wind speed occurred during this period compared to rest of the year. These strong winds generate strong turbulence in the surface water, which enhances vertical mixing.

Deleted: °

Deleted: °

Deleted: °

Deleted: °

Deleted: ¶

3.3 Impact of the eddies¶

Satellite altimetry maps revealed the presence of multiple eddies in the Red Sea which are often confined to specific latitude bands. Quadfasel and Baudner (1993) reported that most of the gyres in the Red Sea are concentrated in four latitude bands, approximately centered on 18° N, 20° N, 23° N and 26.5° N, and some of these eddies are semi-permanent in nature. Johns et al. (1999) also reported the presence of cyclonic eddies in the north and south of the Red Sea and anticyclonic eddies in the central Red Sea. Clifford et al. (1997) and Sofianos and Johns (2007) reported the presence of a quasi-permanent cyclonic gyre in the northern Red Sea during the winter. Analyzing the SLA maps from 1992 to 2012, Zhan et al., (2014) reported the presence of multiple eddies with both polarities in the Red Sea. The number of identified eddies peaked at approximately 19.5° N and 23.5° N. The upwelling proxy constructed using MODIS SST in the northern Red Sea shows the presence of frequent upwelling events at approximately 26.5° N almost every year (Papadopoulos et al., 2015) indicating the presence of cyclonic eddy. The extent and time of the upwelling vary from year to year. ¶

The eddy distribution in the Red Sea for the period from 1992-2012, based on SLA data is given in Fig. 7, where the eddies are identified using the "winding-angle" method (Zhan et al., 2014). The number of eddies are relatively higher in the central and northern Red Sea. The change in vertical stratification due to the presence of anticyclonic eddy (AE) and cyclonic eddy (CE) for different seasons are shown in Fig. 8. The black (green) colored curve represent the profile before (during) the eddy event. The date of profiling is given in the figure caption and the stations are marked. Figure 7a & 7f shows that the presence of AE during spring transformed the completely stratified upper layer to be well mixed till 50 m depth. Similar instance is shown in Fig. 8b & 8g where MLD changed from nearly zero to 30 m during summer. Figure 7c & 7h show the profiles corresponding to a CE event during fall, where shoaling of MLD by ~10 m is observed. Similarly, the CE event during winter lead to shoaling of mixed layer by ~60 m (Fig. 8d & 8i). Figure 8e & 8j show three profiles from single cruise collected within 12 hours which is coincided with the presence of CE and AE in a short distance, in which station A is located outside the AE, B is located inside AE and C is partly in CE. There is a difference of ~100 m in the MLD due to the presence of eddies, in a short distance. Similarly, the MLD at station C is shallower than that of A due to the presence of a CE. ¶

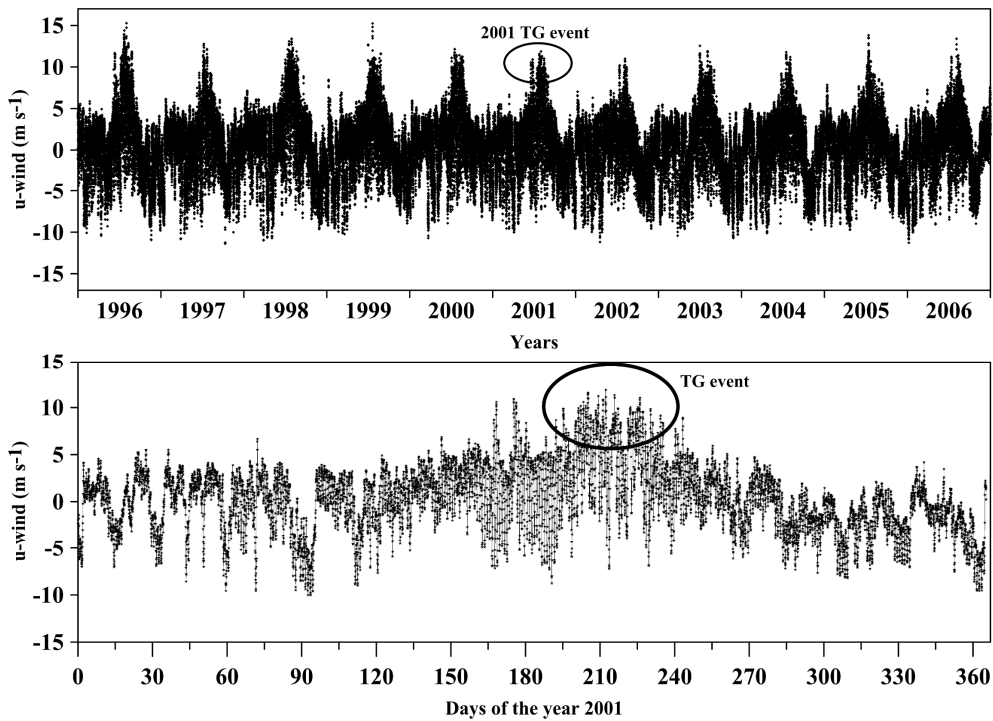
Previous studies have proved that the upper ocean is efficiently re-stratified by the ocean eddies which may significantly change the MLD. The resultant effect of eddy is largely dependent on the eddy amplitude. The mixing intensity is largest at the center of eddy and decays on average with increasing radial distance (Dewar, 1986; Fox-Kemper et al., 2008; Hausmann et al., 2017; Smith and ... [1]

Deleted: 4

Deleted: °

Deleted: 8

Deleted: 8



467

468 **Figure 7.** U-component of the CFSR hourly surface wind near the Tokar region (38.5°E , 18.5°N) a) from
 469 year 1996 to 2006 and b) for the year 2001. The ellipse indicates the TG event in the year 2001.

470 The temperature and salinity profiles measured during summer 2001 (13-14 Aug 2001), which coincided
 471 with the Tokar event are shown in Fig. 8a-b (Sofianos and Johns, 2007; Zhai and Bower, 2013). The
 472 signature of Tokar event is clearly visible in the satellite-derived SLA, with well-defined cyclonic and
 473 anticyclonic eddies to the north and south of the Tokar gap respectively (Fig. 8c-e). Both eddies have
 474 basin-wide influence and radii between 70-80 km. Corresponding wind speed pattern (averaged for the
 475 previous 7 days) is shown (Fig. 8f-h). The profiles to the north and south of the jet axis display a
 476 significant difference in MLD, with a deeper mixed layer in the south. Station A is far from both cyclonic

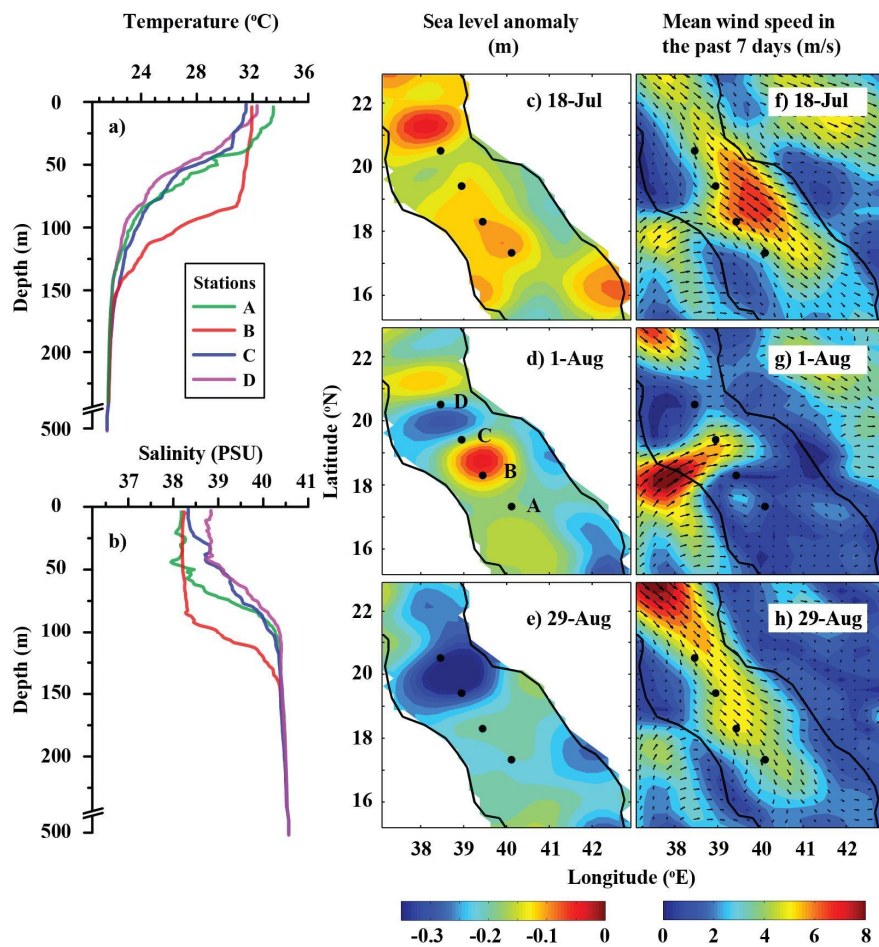
Deleted: 9
 Deleted: °
 Deleted: °

Deleted: 10

Deleted: 10

Deleted: 10

483 and anticyclonic eddies and shows the expected MLD during this period. The presence of the anticyclonic
484 eddy at station B enhances strong downwelling, extending the mixing to a depth of approximately 80 m.
485 It is to be noted that the entire Red Sea basin is well stratified during this period, with MLDs ranging
486 from 10 m to 15 m. Stations C and D are located at the edge of the cyclonic eddy, and both have shallower
487 thermocline and mixed layer.



488

489 **Figure 8.** (a) The CTD measured temperature and salinity profiles during 13-14 Aug 2001. (b) SLA maps
 490 and (c) wind speed and direction (averaged for the previous one week) in the Tokar region, before, during
 491 and after the Tokar event. The temperature and salinity profiles are received through personal
 492 communication from (Sofianos and Johns, 2007).

Deleted: 10

494 The MLDs of all the available profiles in the Tokar region before, during, just after and after a month of
495 the Tokar event are plotted in Fig. 9 (profiles for the first 15 days of each month are displayed). The mean
496 MLD, standard deviation and number of profiles are given in Table 1. Before the Tokar event, the southern
497 and northern sides of the Tokar axis (18°N - 19.5°N and 19.5°N - 21°N , respectively) displayed similar
498 mixed layers (Fig. 9a-c). During the Tokar event, the southern side experienced enhanced mixing, while
499 the northern side show shallow mixed layer (Fig. 9d-f).

Deleted: 11

Deleted: °

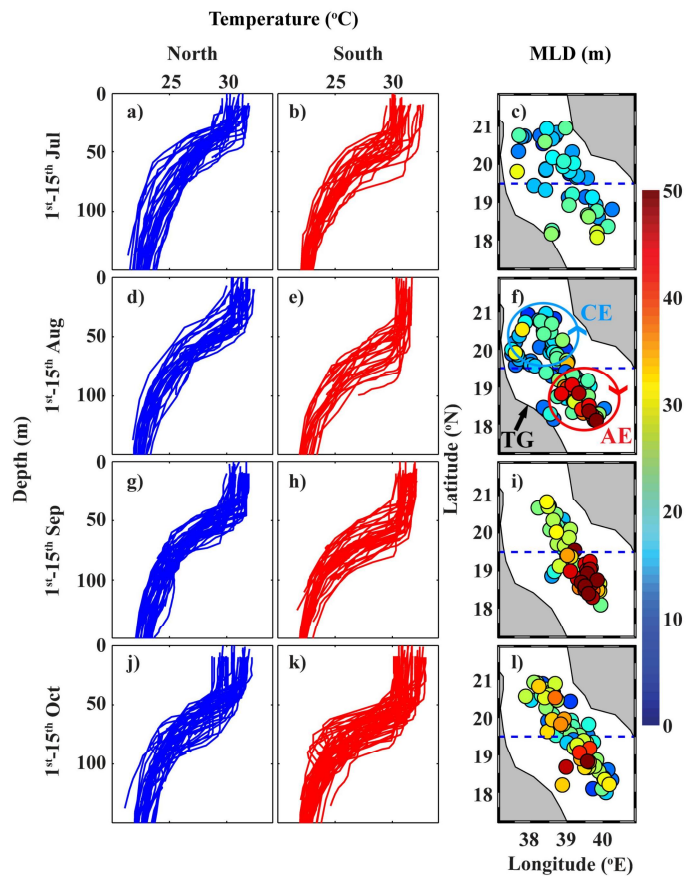
Deleted: °

Deleted: °

Deleted: °

Deleted: 11

Deleted: 11



507

508 **Figure 2.** Temperature profiles from the north of the Tokar axis (left panel, blue curves), south of the
 509 Tokar axis (middle panel, red curves) and the corresponding MLD (right panel) during the first 15 days
 510 of each month from July to October. The dashed line passes through 19.5°N, roughly separating the north
 511 and south of the Tokar axis. MLD of each profile is represented by the filled colors. The blue and red
 512 circles in (f) schematically represent cyclonic and anticyclonic eddies during Tokar event, respectively.

Deleted: 11

Deleted: °

515 **Table 1.** The mean MLD in the north and south of Tokar jet axis from July to October.

1-15 th days of the Month	Mean		Standard deviation		Number of profiles	
	North	South	north	south	north	south
Jul (before)	20	26	5	8	19	12
Aug (during)	24	38	8	17	27	24
Sep (just after)	30	52	11	14	27	27
Oct (after one month)	31	34	9	12	36	30

516 The anticyclonic part of the Tokar induced eddies enhances downwelling and the associated deepening
 517 of the mixed layer along the southern side of the jet axis, while the cyclonic eddies generate upwelling
 518 and the associated shoaling of the mixed layer along the northern side. The profiles in September (just
 519 after the Tokar event) show the southern side is well mixed by the event, which leads to an average
 520 difference of 20 m in the MLDs between both sides of the Tokar axis (Fig. 9g-i). The signature of the
 521 Tokar events in the MLDs (MLD difference between north and south of the jet axis) has disappeared by
 522 October (one month after the Tokar event, Fig. 9j-l). The dominant effect of mountain gap winds on MLD
 523 changes has been reported in many studies globally, for instance, Gulfs of Tehuantepec in the Eastern
 524 Tropical Pacific (Gonzalez-Silvera et al., 2004; Stumpf, 1975) and Bora in the Mediterranean Sea
 525 (Grisogono and Belusic, 2009).

Deleted: 11

Deleted: 11

528 The mixing in the Tokar region during summer is the sum of the two mechanisms, the wind-induced
529 turbulent mixing and the secondary circulation (eddies) induced by the wind. Both mechanisms act in the
530 same direction in the southern side of the jet axis resulting in enhanced mixing, while they act in opposite
531 direction in the northern side leading to reduced mixing. Further studies are required for proper
532 quantification of the contribution of each mechanism. In summary, during the summer, the turbulence
533 induced by strong wind and the impact of anticyclonic eddy enhance vertical mixing in the southern side
534 of jet axis, while the wind-induced mixing is diminished by the presence of cyclonic eddy in the northern
535 side of the jet axis.

536 **4 Conclusions**

537 A detailed information on MLD variability is crucial for understanding the physical and biological
538 processes in the ocean. The goals of this study were to produce a climatology record of MLD for the Red
539 Sea and to investigate the role of major forces on MLD changes. With the help of in situ temperature
540 profiles from CTD, XBT, MBT and profiler float measurements, the MLD variability in the Red Sea has
541 been explored for the first time and the MLD climatology is produced for every 0.5 degrees along the
542 main axis. The climatology reasonably captured all the major features of MLD variability in the Red Sea.
543 The present work provides a climatological mean of the MLD structure in the Red Sea and its seasonal
544 variability. Influences of wind stress, heat flux, evaporation and precipitation are explored. Further, the
545 impact of the Tokar gap jet stream winds, the eddies and the upwelling events in the northern Red Sea are
546 investigated.

547 A deep ventilation process associated with the winter cooling is observed across the entire Red Sea during
548 the months of December to February (Fig. 3). Similarly, very shallow MLDs associated with increased
549 short-wave radiation are detected all along the region from May to Jun. The climatological winter MLD
550 ranges from ~40 to 85 m (in January). Similarly, the climatological summer MLD varies from 10 to ~20
551 m (in June), which may reach to >40 (in July). The mixed layer becomes deeper toward the north, even
552 though the pattern is not linear with increasing latitude. The largest amplitude of variability is observed
553 at the tip of the northern Red Sea which is associated with strong deep convection during the winter and

554 shoaling during the summer. The region at approximately 19°N experienced deeper MLD than typical of
555 elsewhere in the Red Sea. This region experienced enhanced mixing during winter by surface cooling,
556 and during summer by both the Tokar gap wind induced turbulent mixing and the formation of the
557 anticyclonic eddy. The deepest mixed layer is observed at the northern tip of Red Sea during the winter,
558 but the deep nature of northern mixed layer is almost limited to the winter months.

Deleted: °

559 Correlation analyses between MLD and forcing factors displayed the influence of major forces on MLD,
560 from north to south of the Red Sea. In general, the wind stress mainly controls the MLD variability in the
561 southern part of the Red Sea, heat flux and evaporation dominate in the central region, and all the three
562 forces contribute in the northern region. Coinciding drops are observed in the correlations for all the
563 selected forcing factors around the previously reported main eddy locations. In these locations, eddies
564 override the controls of the other main forces, namely, wind stress, heat flux and fresh-water flux. The
565 quasi-permanent cyclonic gyre and upwelling in the northern Red Sea lead to the shoaling of the mixed
566 layer at ~26.5°N throughout almost the whole year.

Deleted: °

567 The anticyclonic eddy induced by Tokar gap winds, and the wind induced turbulent mixing together
568 enhanced the deep convection and mixing along the southern side of the Tokar jet axis during the summer,
569 while the wind induced mixing is reduced by the cyclonic eddy. This leads to a deepening of the mixed
570 layer, to >40 m, while the MLDs in the rest of the Red Sea are <20 m. The effect of Tokar event is seen
571 in the profiles of late July to early August which gradually disappeared by October. The frequent eddies,
572 associated with surface circulation and Tokar events, have a strong impact on the MLD structure of the
573 Red Sea.

574 **Data availability**

575 The climatology data produced in this manuscript is available from the repository "Figshare"
576 (DOI:10.6084/m9.figshare.5539852). The monthly mean values of heat fluxes and wind stress data are
577 available from Tropflux (http://www.incois.gov.in/tropflux_datasets/data/monthly/). The monthly mean
578 values of evaporation are accessible from OAflux

581 (ftp://ftp.who.edu/pub/science/oaflux/data_v3/monthly/evaporation/). The precipitation data is available
582 from TRMM (<https://pmm.nasa.gov/data-access/downloads/trmm>).

583 **Acknowledgments**

584 This project was funded by the Deanship of Scientific Research (DSR), King Abdulaziz University, under
585 grant number (438/150/129). The authors, therefore, acknowledge the DSR's technical and financial
586 support. The authors acknowledge TropFlux, OAFflux, TRMM, AVISO, CFSR, World Ocean Database
587 and Coriolis data center for making their data products publicly available. The authors also acknowledge
588 the institutes who have provided CTD profiles from different cruises. The author CPA acknowledges the
589 Deanship of Graduate Studies, King Abdulaziz University, Jeddah, for providing a Ph.D. Fellowship.

590 **References**

591

592

593 Abdulla, C. P., Alsaafani, M. A., Alraddadi, T. M. and Albarakati, A. M.: Estimation of Mixed Layer
594 Depth in the Gulf of Aden: A New Approach, PLoS One, 11(10), e0165136,
595 doi:10.1371/journal.pone.0165136, 2016.

596 Aboobacker, V. M., Shanas, P. R., Alsaafani, M. A. and Albarakati, A. M.: Wave energy resource
597 assessment for Red Sea, Renew. Energy, 1–13, doi:10.1016/j.renene.2016.09.073, 2016.

598 Albarakati, A. M. and Ahmad, F.: Variation of the surface buoyancy flux in the Red Sea, Indian J. Mar.
599 Sci., 42(6), 717–721, 2013.

600 Alsaafani, M. A. and Shenoi, S. S. C.: Seasonal cycle of hydrography in the Bab el Mandab region,
601 southern Red Sea, J. Earth Syst. Sci., 113(3), 269–280, doi:10.1007/BF02716725, 2004.

602 Alsaafani, M. A. and Shenoi, S. S. C.: Water masses in the Gulf of Aden, *J. Oceanogr.*, 63(1), 1–14,
603 doi:10.1007/s10872-007-0001-1, 2007.

604 Beal, L. M., Field, A. and Gordon, A. L.: Spreading of Red Sea overflow waters in the Indian Ocean, *J.*
605 *Geophys. Res.*, 105(C4), 8549–8564, doi:10.1029/1999JC900306, 2000.

606 Bower, A. S. and Farrar, J. T.: Air-sea interaction and horizontal circulation in the Red Sea, in *The Red*
607 *Sea*, pp. 329–342, Springer., 2015.

608 Boyer, T. P. and Levitus, S.: Quality control and processing of historical temperature, salinity, and
609 oxygen data, NOAA Tech. Rep., NESDIS 81, 65, 1994.

610 de Boyer Montegut, C., Madec, G., Fischer, A. S., Lazar, A. and Iudicone, D.: Mixed layer depth over
611 the global ocean: An examination of profile data and a profile-based climatology, *J. Geophys. Res. C*
612 *Ocean.*, 109(12), 1–20, doi:10.1029/2004JC002378, 2004.

613 Bretherton, C. S., Widmann, M., Dymnikov, V. P., Wallace, J. M. and Bladé, I.: The Effective Number
614 of Spatial Degrees of Freedom of a Time-Varying Field, *J. Clim.*, 12(7), 1990–2009, doi:10.1175/1520-
615 0442(1999)012<1990:TENOSD>2.0.CO;2, 1999.

616 Carlson, D. F., Fredj, E. and Gildor, H.: The annual cycle of vertical mixing and restratification in the
617 Northern Gulf of Eilat/Aqaba (Red Sea) based on high temporal and vertical resolution observations,
618 *Deep. Res. Part I Oceanogr. Res. Pap.*, 84, 1–17, doi:10.1016/j.dsr.2013.10.004, 2014.

619 Chelton, D. B., Schlax, M. G., Freilich, M. H. and Milliff, R. F.: Satellite measurements reveal
620 persistent small-scale features in ocean winds, *Science* (80-.), 303(5660), 978–983, 2004.

621 Chelton, D. B., Schlax, M. G. and Samelson, R. M.: Global observations of nonlinear mesoscale eddies,
622 *Prog. Oceanogr.*, 91(2), 167–216, doi:10.1016/j.pocean.2011.01.002, 2011.

- 623 Chen, D., Busalacchi, A. J. and Rothstein, L. M.: The roles of vertical mixing, solar radiation, and wind
624 stress in a model simulation of the sea surface temperature seasonal cycle in the tropical Pacific Ocean,
625 *J. Geophys. Res.*, 99(C10), 20345, doi:10.1029/94JC01621, 1994.
- 626 Cheng, L., Zhu, J., Cowley, R., Boyer, T. P. and Wijffels, S.: Time, probe type, and temperature
627 variable bias corrections to historical expendable bathythermograph observations, *J. Atmos. Ocean.
628 Technol.*, 31(8), 1793–1825, doi:10.1175/JTECH-D-13-00197.1, 2014.
- 629 Clifford, M., Horton, C., Schmitz, J. and Kantha, L. H.: An oceanographic nowcast/forecast system for
630 the Red Sea, *J. Geophys. Res. Ocean.*, 102(C11), 25101–25122, doi:10.1029/97JC01919, 1997.
- 631 D’Ortenzio, F., Iudicone, D., de Boyer Montegut, C., Testor, P., Antoine, D., Marullo, S., Santoleri, R.
632 and Madec, G.: Seasonal variability of the mixed layer depth in the Mediterranean Sea as derived from
633 in situ profiles, *Geophys. Res. Lett.*, 32(12), L12605, doi:10.1029/2005GL022463, 2005.
- 634 Dewar, W. K.: Mixed layers in Gulf Stream rings, *Dyn. Atmos. Ocean.*, 10(1), 1–29, 1986.
- 635 Ducet, N., LaTraon, P. Y. and Reverdin, G.: Global high-resolution mapping of ocean circulation from
636 TOPEX/Poseidon and ERS-1 and -2, *J. Geophys. Res. Ocean.*, 105(C8), 19477–19498,
637 doi:10.1029/2000JC900063, 2000.
- 638 Fox-Kemper, B., Ferrari, R. and Hallberg, R.: Parameterization of Mixed Layer Eddies. Part I: Theory
639 and Diagnosis, *J. Phys. Oceanogr.*, 38(6), 1145–1165, doi:10.1175/2007JPO3792.1, 2008.
- 640 Gonzalez-Silvera, A., Santamaria-del-Angel, E., Millán-Nuñez, R. and Manzo-Monroy, H.: Satellite
641 observations of mesoscale eddies in the Gulfs of Tehuantepec and Papagayo (Eastern Tropical Pacific),
642 *Deep Sea Res. Part II Top. Stud. Oceanogr.*, 51(6–9), 587–600, doi:10.1016/j.dsr2.2004.05.019, 2004.
- 643 Grisogono, B. and Belusic, D.: A review of recent advances in understanding the meso- and microscale

644 properties of the severe Bora wind, *Tellus A*, 61(1), 1–16, doi:10.1111/j.1600-0870.2008.00369.x,
645 2009.

646 Hausmann, U., McGillicuddy, D. J. and Marshall, J.: Observed mesoscale eddy signatures in Southern
647 Ocean surface mixed-layer depth, *J. Geophys. Res. Ocean.*, 122(1), 617–635,
648 doi:10.1002/2016JC012225, 2017.

649 Jiang, H., Farrar, J. T., Beardsley, R. C., Chen, R. and Chen, C.: Zonal surface wind jets across the Red
650 Sea due to mountain gap forcing along both sides of the Red Sea, *Geophys. Res. Lett.*, 36(19), 1–6,
651 doi:10.1029/2009GL040008, 2009.

652 Johns, W. E., Jacobs, G. A., Kindle, J. C., Murray, S. P. and Carron, M.: Arabian marginal seas and
653 gulfs. University of Miami RSMAS Technical Report., University of Miami, Florida, USA., 1999.

654 Kara, A. B., Rochford, P. A. and Hurlburt, H. E.: Mixed layer depth variability over the global ocean, *J.*
655 *Geophys. Res.*, 108(C3), 3079, doi:10.1029/2000JC000736, 2003.

656 Keerthi, M. G., Dyn, C., Monte, C. D. B., Lengaigne, M., Vialard, J., Boyer Montégut, C.,
657 Muraleedharan, P. M., Dyn, C., Monte, C. D. B., Keerthi, M. G., Lengaigne, M., Vialard, J., Boyer
658 Montégut, C., Muraleedharan, P. M., de Boyer Montégut, C. and Muraleedharan, P. M.: Interannual
659 variability of the Tropical Indian Ocean mixed layer depth, *Clim. Dyn.*, 40(3–4), 743–759,
660 doi:10.1007/s00382-012-1295-2, 2012.

661 Keerthi, M. G., Lengaigne, M., Drushka, K., Vialard, J., Montegut, C. D. B., Pous, S., Levy, M. and
662 Muraleedharan, P. M.: Intraseasonal variability of mixed layer depth in the tropical Indian Ocean, *Clim.*
663 *Dyn.*, 46(7–8), 2633–2655, doi:10.1007/s00382-015-2721-z, 2016.

664 LaTraon, P. Y. and Dibarboure, G.: Mesoscale Mapping Capabilities of Multiple-Satellite Altimeter
665 Missions, *J. Atmos. Ocean. Technol.*, 16(9), 1208–1223, doi:10.1175/1520-

666 0426(1999)016<1208:MMCOMS>2.0.CO;2, 1999.

667 Lorbacher, K., Dommenget, D., Niiler, P. P. and Köhl, A.: Ocean mixed layer depth: A subsurface
668 proxy of ocean-atmosphere variability, *J. Geophys. Res. Ocean.*, 111(7), 1–22,
669 doi:10.1029/2003JC002157, 2006.

670 Papadopoulos, V. P., Zhan, P., Sofianos, S. S., Raitzos, D. E., Qurban, M., Abualnaja, Y., Bower, A. S.,
671 Kontoyiannis, H., Pavlidou, A., Asharaf, T. T. M., Zarokanellos, N. and Hoteit, I.: Factors governing
672 the deep ventilation of the Red Sea, *J. Geophys. Res. Ocean.*, 120(11), 7493–7505,
673 doi:10.1002/2015JC010996, 2015.

674 Polovina, J., Mitchum, G. T. and Evans, T.: Decadal and basin-scale variation in mixed layer depth and
675 the impact on biological production in the Central and North Pacific , 1960-88, *Deep Sea Res.*, 42(10),
676 1701–1716, 1995.

677 Praveen Kumar, B., Vialard, J., Lengaigne, M., Murty, V. S. N. and McPhaden, M. J.: TropFlux: air-sea
678 fluxes for the global tropical oceans—description and evaluation, *Clim. Dyn.*, 38(7–8), 1521–1543,
679 doi:10.1007/s00382-011-1115-0, 2012.

680 Praveen Kumar, B., Vialard, J., Lengaigne, M., Murty, V. S. N., McPhaden, M. J., Cronin, M. F.,
681 Pinsard, F. and Gopala Reddy, K.: TropFlux wind stresses over the tropical oceans: evaluation and
682 comparison with other products, *Clim. Dyn.*, 40(7–8), 2049–2071, doi:10.1007/s00382-012-1455-4,
683 2013.

684 Quadfasel, D. and Baudner, H.: Gyre-scale circulation cells in the red-sea, *Oceanol. Acta*, 16(3), 221–
685 229, 1993.

686 Ralston, D. K., Jiang, H. and Farrar, J. T.: Waves in the Red Sea: Response to monsoonal and mountain
687 gap winds, *Cont. Shelf Res.*, 65, 1–13, doi:10.1016/j.csr.2013.05.017, 2013.

688 Saha, S., Moorthi, S., Pan, H. L., Wu, X., Wang, J., Nadiga, S., Tripp, P., Kistler, R., Woollen, J.,
689 Behringer, D., Liu, H., Stokes, D., Grumbine, R., Gayno, G., Wang, J., Hou, Y. T., Chuang, H. Y.,
690 Juang, H. M. H., Sela, J., Iredell, M., Treadon, R., Kleist, D., Van Delst, P., Keyser, D., Derber, J., Ek,
691 M., Meng, J., Wei, H., Yang, R., Lord, S., Van Den Dool, H., Kumar, A., Wang, W., Long, C.,
692 Chelliah, M., Xue, Y., Huang, B., Schemm, J. K., Ebisuzaki, W., Lin, R., Xie, P., Chen, M., Zhou, S.,
693 Higgins, W., Zou, C. Z., Liu, Q., Chen, Y., Han, Y., Cucurull, L., Reynolds, R. W., Rutledge, G. and
694 Goldberg, M.: The NCEP climate forecast system reanalysis, *Bull. Am. Meteorol. Soc.*, 91(8), 1015–
695 1057, doi:10.1175/2010BAMS3001.1, 2010.

696 Shanas, P. R., Aboobacker, V. M., Albarakati, A. M. A. and Zubier, K. M.: Climate driven variability of
697 wind-waves in the Red Sea, *Ocean Model.*, 119, 105–117, doi:10.1016/j.ocemod.2017.10.001, 2017.

698 Smith, K. S. and Marshall, J.: Evidence for Enhanced Eddy Mixing at Middepth in the Southern Ocean,
699 *J. Phys. Oceanogr.*, 39(1), 50–69, doi:10.1175/2008JPO3880.1, 2009.

700 Sofianos, S. S. and Johns, W. E.: An Oceanic General Circulation Model (OGCM) investigation of the
701 Red Sea circulation, 1. Exchange between the Red Sea and the Indian Ocean, *J. Geophys. Res.*,
702 107(C11), 3196, doi:10.1029/2001JC001184, 2002.

703 Sofianos, S. S. and Johns, W. E.: Observations of the summer Red Sea circulation, *J. Geophys. Res.*
704 *Ocean.*, 112(6), 1–20, doi:10.1029/2006JC003886, 2007.

705 Sofianos, S. S., Johns, W. E. and Murray, S. P.: Heat and freshwater budgets in the Red Sea from direct
706 observations at Bab el Mandeb, *Deep. Res. Part II Top. Stud. Oceanogr.*, 49(7–8), 1323–1340,
707 doi:10.1016/S0967-0645(01)00164-3, 2002.

708 Stumpf, H. G.: Satellite Detection of Upwelling in the Gulf of Tehuantepec, Mexico, *J. Phys.*
709 *Oceanogr.*, 5(2), 383–388, doi:10.1175/1520-0485(1975)005<0383:SDOUIT>2.0.CO;2, 1975.

710 Sutton, P. J., Worcester, P. F., Masters, G., Cornuelle, B. D. and Lynch, J. F.: Ocean mixed layers and
711 acoustic pulse propagation in the Greenland Sea, *J Acoust Soc Am*, 94(3), 1517–1526,
712 doi:10.1121/1.408130, 2014.

713 Tragou, E., Garrett, C., Outerbridge, R. and Gilman, C.: The Heat and Freshwater Budgets of the Red
714 Sea, *J. Phys. Oceanogr.*, 29(10), 2504–2522, doi:10.1175/1520-
715 0485(1999)029<2504:THAFBO>2.0.CO;2, 1999.

716 Turner, J. S.: *Buoyancy Effects in Fluids*, Cambridge University Press, Cambridge., 1973.

717 Yao, F., Hoteit, I., Pratt, L. J., Bower, A. S., Zhai, P., Köhl, A. and Gopalakrishnan, G.: Seasonal
718 overturning circulation in the Red Sea: 1. Model validation and summer circulation, *J. Geophys. Res.*
719 *Ocean.*, 119(4), 2238–2262, doi:10.1002/2013JC009004, 2014a.

720 Yao, F., Hoteit, I., Pratt, L. J., Bower, A. S., Köhl, A., Gopalakrishnan, G. and Rivas, D.: Seasonal
721 overturning circulation in the Red Sea: 2. Winter circulation, *J. Geophys. Res. Ocean.*, 119(4), 2263–
722 2289, doi:10.1002/2013JC009331, 2014b.

723 Zeng, L. and Wang, D.: Seasonal variations in the barrier layer in the South China Sea: characteristics,
724 mechanisms and impact of warming, *Clim. Dyn.*, 48(5–6), 1911–1930, doi:10.1007/s00382-016-3182-
725 8, 2017.

726 Zhai, P. and Bower, A. S.: The response of the Red Sea to a strong wind jet near the Tokar Gap in
727 summer, *J. Geophys. Res. Ocean.*, 118(1), 422–434, doi:10.1029/2012JC008444, 2013.

728 Zhan, P., Subramanian, A. C., Yao, F. and Hoteit, I.: Eddies in the Red Sea: A statistical and dynamical
729 study, *J. Geophys. Res. Ocean.*, 119(6), 3909–3925, doi:10.1002/2013JC009563, 2014.

730